Journal of Geospatial Science and Technology, 2026
6(1), 91-105, DOI: https://doi.org/10.xxxx/xxxx

Geospatial Assessment of Urban Heat Island and Climate Dynamics in Ile Ife, Southwest Nigeria

A. M. Adesiyan[1*], S.O. Akande[2], J. Oloukoi[1]

[1]*African Regional Institute for Geospatial Information Science and Technology (AFRIGIST), Obafemi Awolowo University, Ile-Ife, Nigeria*
[2]*Federal University of Technology, Akure, Nigeria*

(Received 29 April 2026; Accepted 20 August 2026; online 23 September 2026)

Abstract

Rapid urban growth can alter surface energy balance and intensify surface urban heat islands (SUHIs), yet secondary cities in sub-Saharan Africa remain comparatively understudied. This study assessed spatiotemporal surface thermal dynamics and local climate variability in Ile-Ife, Nigeria, using Landsat scenes acquired on 15 January 1986, 3 January 2002 and 25 December 2024, MODIS MOD11A2 land surface temperature (LST) data for 2000–2024 and CHIRPS rainfall data for 1986–2024. Land use/land cover (LULC), Normalized Difference Vegetation Index (NDVI), Normalized Difference Built-up Index (NDBI), LST and long-term temperature trends were analysed. Built-up land increased from 18.20 km² in 1986 to 106.27 km² in 2024, while vegetation declined from 359.52 km² to 251.92 km². Built-up surfaces were consistently warmer than vegetation, with built-up-minus-vegetation surface thermal contrasts of 7.98 °C, 4.21 °C, and 7.51 °C in 1986, 2002 and 2024, respectively. NDVI was negatively associated with LST ($r = -0.18, -0.85$ and -0.90), whereas NDBI was positively associated with LST ($r = 0.62, 0.88$, and 0.90). The 2000–2024 MODIS series showed a significant warming trend (Mann–Kendall $Z = 3.67$, $p = 0.00025$, Sen's slope = 0.0759 °C/year). Rainfall varied substantially but was analysed as climatic context rather than as an independently estimated causal driver. The combined evidence indicates persistent surface warming associated with rapid built-up expansion and vegetation loss, supporting the need for heat-sensitive land-use planning, vegetation protection, and targeted green infrastructure in Ile-Ife.

Keywords: Surface Urban Heat Island, Land Surface Temperature, Land Use/Land Cover, NDVI, NDBI, Remote Sensing

1. Introduction

Urbanization is reshaping land cover and local climate in cities worldwide. The United Nations estimates that 55% of the global population lived in urban areas in 2018 and projected this proportion to reach 68% by 2050 (United Nations, 2019). Replacing vegetated and permeable surfaces with buildings, roads, and other impervious materials alters surface energy exchange, reduces evapotranspiration, increases heat storage, and contributes to urban overheating (Santamouris, 2020). Urban heat islands can be examined through near-surface air temperature or through satellite-derived land surface temperature (LST). Because the present analysis is based primarily on thermal remote

*Corresponding author. Email: mademola421@gmail.com
†Present address: African Regional Institute for Geospatial Information Science and Technology (AFRIGIST), Obafemi Awolowo University, Ile-Ife, Nigeria.

sensing, the surface expression of the phenomenon is more precisely described as a surface urban heat island (SUHI) (Voogt & Oke, 2003; Zhou et al., 2019). Landsat provides spatial detail suitable for intra-urban analysis, whereas MODIS offers a denser temporal record for examining longer-term LST variability. Spectral indices such as NDVI and NDBI further help characterize the vegetation and built-up patterns associated with surface temperature (Weng et al., 2004; Zha et al., 2003).

Evidence from tropical African cities indicates that rapid land-cover transformation can intensify surface warming. In Lagos, Ayanlade (2017) reported higher LST in urban areas than in surrounding rural areas and linked the pattern to dense development and limited vegetation. In Greater Accra, Wemegah et al. (2020) found increasing UHI spatial coverage and stronger warming over built-up and bare surfaces. These studies demonstrate the value of integrating land-cover and thermal information, but comparatively fewer long-term assessments focus on secondary or historically important cities.

Ile-Ife is a rapidly changing secondary city in southwestern Nigeria where urban expansion has occurred alongside substantial modification of vegetation and open land. Its scale and development pattern differ from those of megacities such as Lagos, making it useful for examining whether the land-cover–temperature relationships commonly reported in larger cities are also evident in a medium-sized urban setting. Long-term analysis is particularly important because single-date thermal imagery can be influenced by short-term weather, soil moisture, atmospheric conditions, and sensor characteristics.

Accordingly, this study examines the spatiotemporal surface thermal dynamics of Ile-Ife using multi-temporal Landsat imagery, MODIS LST, and CHIRPS rainfall data. The objectives are to: (i) characterize LST patterns in 1986, 2002, and 2024; (ii) quantify LULC change and the spatial associations of LST with NDVI and NDBI; and (iii) assess the 2000–2024 MODIS LST trend while interpreting rainfall variability as local climate context. Throughout the paper, “SUHI” or “surface thermal contrast” is used when referring specifically to satellite-derived surface temperature differences, while “UHI” is retained for the broader urban-climate concept.

2. Materials and Methods

2.1 Study area

The analysis covers approximately 491.5 km² centred on Ile-Ife, southwestern Nigeria. The mapped extent is approximately 7.40°–7.60° N and 4.45°–4.65° E and includes urban, peri-urban, agricultural, bare, water and vegetated surfaces. The area has a tropical wet-and-dry climate, with a pronounced rainy season and substantial interannual rainfall variability. Relief is generally undulating and drainage channels and low-lying areas contribute to spatial differences in moisture and surface temperature (Figure 1).

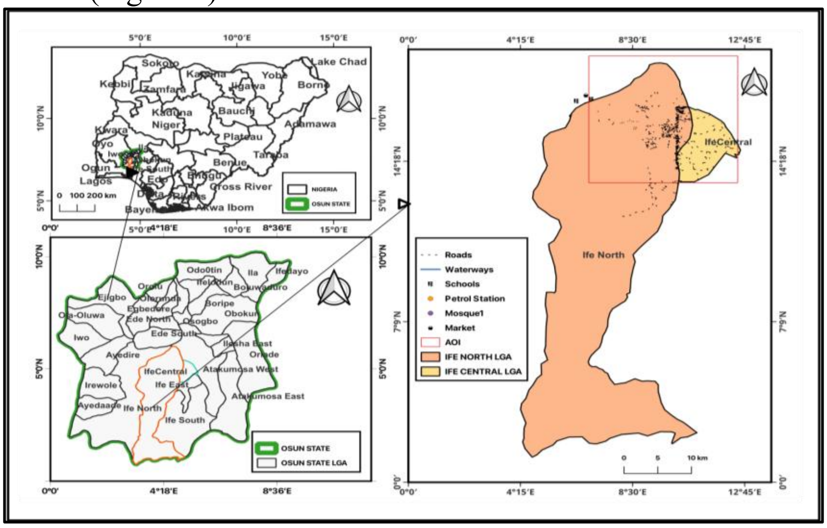

Figure 1. Location and analysis boundary of the Ile-Ife study area.

2.2 Data

The Landsat benchmark scenes were selected from a comparable dry-season window to reduce seasonal contrast: 15 January 1986, 3 January 2002 and 25 December 2024. MOD11A2 was used for the annual 2000–2024 LST time series because its 8-day composites provide substantially greater temporal density than Landsat. CHIRPS supplied a spatially continuous rainfall record for 1986–2024. The datasets and their roles are summarized in Table 1.

Table 1. Characteristics of datasets used in the study.

S/N	Data Type	Acquisition Date / Period	Resolution	Source	Use in Study
1	Landsat TM, ETM+, OLI/TIRS	15 Jan 1986; 3 Jan 2002; 25 Dec 2024	30 m optical; thermal data processed to the common analysis grid	USGS	LULC classification, indices, and LST retrieval
2	MODIS LST (MOD11A2)	2000–2024	1 km; 8-day composite	NASA LP DAAC	Long-term LST time series and trend analysis
3	CHIRPS rainfall	1986–2024	0.05° (~5 km)	CHC / UCS B	Rainfall variability and climate context
4	Administrative b oundaries	2024	1:50,000	OSM / Surveyor General	Study-area delineation

2.3 Image preprocessing and LULC classification

Satellite images were radiometrically preprocessed, cloud and cloud-shadow pixels were excluded using quality-assurance information and all raster layers were projected, clipped, and aligned to a common analysis extent. Sensor-specific scaling information from scene metadata was used during thermal conversion. The use of consistent spatial alignment was essential for pixel-level comparison across LST, NDVI, NDBI and LULC products (Chander et al., 2009; Vermote et al., 2016).

LULC was classified into vegetation, built-up land, waterbody and bare land using supervised maximum-likelihood classification. Reference samples were derived from contemporaneous or historically appropriate imagery and ancillary information. Classification accuracy was assessed with independent validation samples and confusion matrices following established remote-sensing accuracy-assessment practice (Congalton & Green, 2019). For each benchmark year, the confusion matrix was used to derive overall accuracy, the Kappa coefficient, and class-level producer's and user's accuracy, so that agreement attributable to chance and any class-specific misclassification (e.g., spectral confusion between bare land and built-up surfaces) can be distinguished from the aggregate accuracy figure. Overall accuracies computed from the validation confusion matrices were 83.00% for 1986, 83.00% for 2002 and 83.00% for 2024. Cohen's Kappa, calculated from the same confusion matrices, was 0.68 for 1986, 0.73 for 2002, and 0.73 for 2024, all indicating substantial agreement beyond chance (Landis & Koch, 1977). Class-level producer's accuracy (recall) and user's accuracy (precision) are reported in Table 2. The 1986 classification used codes 1 = Vegetation, 20 = Built-Up, 29 = Waterbody, and 31 = Bare Land; the 2024 classification used codes 1 = Vegetation, 22 = Built-Up, 51 = Waterbody, and 44 = Bare Land; the 2002 assessment used codes 1 = Vegetation, 2 = Built-Up, 3 = Bare Land, and 4 = Waterbody. In 1986, producer's accuracy was low for two minority classes (Built-Up: 37.5%; Waterbody: 14.3%) despite high user's accuracy for those classes (100%). This indicates that validation points for these classes were frequently classified into a majority class even though pixels predicted as these classes were reliable; this reflects the small validation sample sizes for these classes (n = 8 and n = 7, respectively) rather than a general classification weakness. In 2002, producer's and user's accuracy were most reliable for vegetation and built-up land (81.4%/94.1% and 87.0%/87.0%, respectively), while the waterbody class had high producer's accuracy (100%) but lower user's accuracy (45.5%), indicating some over-prediction of waterbody in that scene, likely reflecting its small validation sample (n = 5). In 2024, producer's and user's accuracy were more balanced across classes, except for the minority Bare Land class (n = 6), for which no validation points were correctly classified (producer's accuracy = 0%) and no pixels were predicted into that class (user's accuracy undefined).

Table 2. Classification accuracy metrics by land use/land cover class, 1986, 2002, and 2024.

Year	Class (code)	Validation n	Producer's accuracy (%)	User's accuracy (%)	Overall accuracy (%)	Kappa
1986	Vegetation (1)	56	100.0	78.9	83.00	0.68
	Built-Up (20)	8	37.5	100.0		
	Waterbody (29)	7	14.3	100.0		
	Bare Land (31)	29	79.3	92.0		
2002	Vegetation	59	81.4	94.1	83.00	0.73
	Built-Up	23	87.0	87.0		
	Waterbody	5	100.0	45.5		
	Bare Land	13	76.9	66.7		
2024	Vegetation (1)	47	97.9	82.1	83.00	0.73
	Built-Up (22)	22	77.3	89.5		
	Waterbody (51)	25	80.0	80.0		
	Bare Land (44)	6	0.0	n/a		

2.4 Spectral indices and LST

LST was retrieved from the Landsat thermal observations using a standard radiance–brightness-temperature–emissivity workflow, following the calibration and retrieval procedures described in Chander et al. (2009) and Vermote et al. (2016) and applied consistently across all three benchmark scenes. Spectral radiance was calculated using Equation (1) (Chander et al., 2009).

$$L_\lambda = M_L \times Q_{cal} + A_L \quad (1)$$

where Lλ is spectral radiance, ML and AL are the multiplicative and additive radiance scaling factors, and Qcal is the calibrated digital number.

At-sensor brightness temperature was then obtained using Equation (2).

$$T_B = \frac{K_2}{ln ln \left[\left(\frac{K_1}{L_\lambda}\right) + 1\right]} \quad (2)$$

where TB is brightness temperature and K1 and K2 are sensor-specific thermal calibration constants.

Surface emissivity correction and conversion to degrees Celsius were applied using Equation (3), following the standard mono-window emissivity-correction approach widely used in Landsat-based LST retrieval (Weng et al., 2004); interpretation of satellite LST as a surface quantity follows Voogt and Oke (2003).

$$LST\ (°C) = \frac{T_B}{1 + \left[\frac{\lambda T_B}{\rho} ln ln\ (\varepsilon)\right]} - 273.15 \quad (3)$$

where λ is the effective wavelength of emitted radiance, ρ = 1.438 × 10⁻² m·K, and ε is land-surface emissivity.

NDVI was calculated using Equation (4) to represent vegetation abundance (Tucker, 1979).

$$NDVI = \frac{NIR - Red}{NIR + Red} \quad (4)$$

NDBI was calculated using Equation (5) to represent built-up spectral response (Zha et al., 2003).

$$NDBI = \frac{SWIR - NIR}{SWIR + NIR} \quad (5)$$

NIR, Red, and SWIR denote the near-infrared, red, and shortwave-infrared reflectance bands appropriate to each Landsat sensor. NDVI and NDBI were calculated from surface-reflectance data and then aligned with the corresponding LST raster for spatial analysis.

2.5 Surface thermal intensity and change

For each benchmark year, LST was mapped and summarized by LULC class. Low, medium, and high thermal classes were generated using equal intervals for within-scene visualization. Because year-specific equal intervals do not constitute a fixed urban–rural reference, these classes are interpreted as relative surface thermal zones rather than directly comparable UHI-intensity thresholds. The mean LST difference between built-up and vegetation classes is therefore reported as a built-up–vegetation surface thermal contrast, not as canopy-layer air-temperature UHI intensity. LST change between 1986 and 2024 was calculated after aligning the rasters to a common extent, projection, and pixel grid. Positive values indicate surface warming and negative values indicate cooling. The three benchmark scenes fall within a similar dry-season window, but scene-specific atmospheric and moisture conditions may still affect direct cross-year comparison.

2.6 Statistical analysis

Pearson's correlation coefficient summarized the bivariate spatial relationships between LST and NDVI and between LST and NDBI for each benchmark scene, based on the full set of valid, cloud-free pixels common to both raster layers in each scene. Sample sizes were n = 555,770 (1986), n = 2,183,000 (2002), and n = 551,803 (2024) for the NDVI–LST pairing, and n = 555,024 (1986), n = 2,183,000 (2002), and n = 551,803 (2024) for the NDBI–LST pairing. The substantially larger 2002 pixel count reflects that the 2002 scene was processed at a finer spatial resolution than the 1986 and 2024 scenes; because the correlation coefficients are computed per pixel pair within each scene rather than pooled across years, this difference in resolution does not bias the within-scene r or R^2 values, but it does mean the 2002 estimate draws on a finer-grained sample and its nominal n is not directly comparable to the other two years. All correlations were statistically significant at two-tailed $p < 0.001$ given these sample sizes. Because neighbouring raster pixels are spatially autocorrelated and the variables were derived from the same satellite scenes, conventional p-values calculated on the nominal pixel count overstate the effective degrees of freedom; the coefficients are therefore interpreted as descriptive spatial associations rather than as independent-sample causal estimates, and readers should treat the nominal significance levels as an upper bound on statistical confidence rather than a formal hypothesis test.

The Mann–Kendall test was applied to the annual MODIS LST series for 2000–2024 to assess a monotonic trend (Mann, 1945). Sen’s slope estimated the median annual rate of change (Sen, 1968). Statistical significance was evaluated at $\alpha = 0.05$. Rainfall was analysed descriptively as climatic context; no independent causal rainfall effect is claimed because a multivariable or lagged attribution model was not fitted.

3. Results

3.1 Land surface temperature patterns

LST varied substantially across the benchmark scenes (Table 3; Figure 2). The observed ranges were 24.27–33.63 °C in 1986, 32.50–38.14 °C in 2002 and 28.63–40.57 °C in 2024. Warmer surfaces were concentrated in the urban core and along expanding development corridors, whereas vegetated areas were generally cooler. The relatively high minimum LST in 2002 indicates that scene-level conditions affect absolute temperature and reinforces the need to interpret the three Landsat dates alongside the longer MODIS series.

Table 3. Summary statistics of Landsat-derived LST in Ile-Ife.

Year	Min LST (°C)	Max LST (°C)
1986	24.27	33.63
2002	32.50	38.14
2024	28.63	40.57

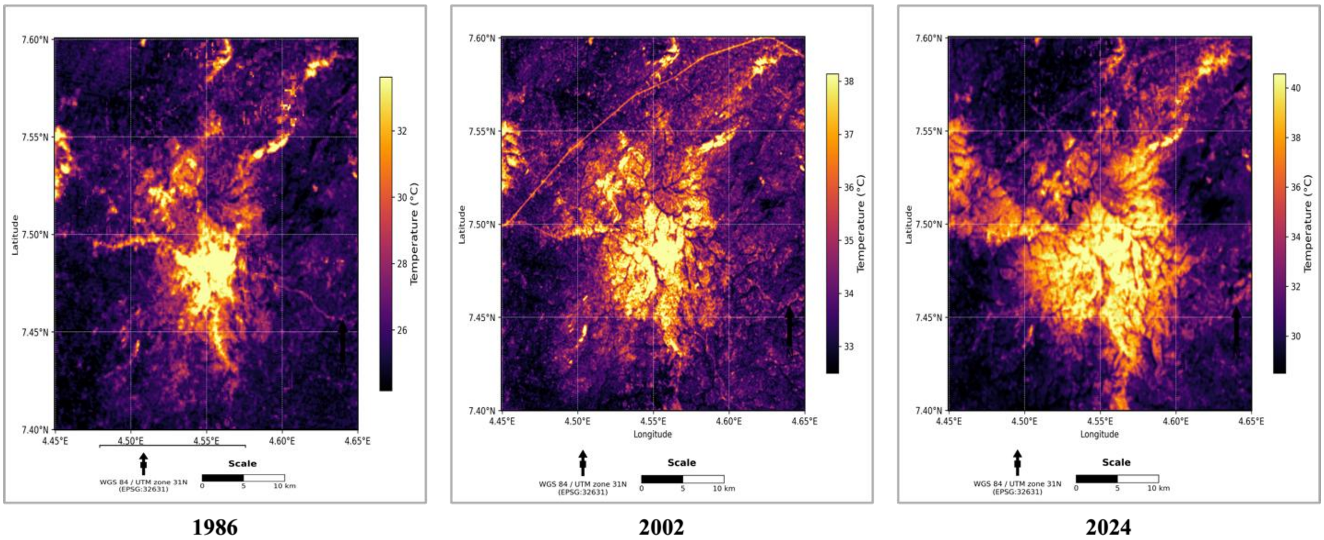

Figure 2. Land surface temperature distribution in 1986, 2002, and 2024.

The 1986–2024 LST change map (Figure 3) ranged from −0.52 °C to +14.75 °C. Positive changes predominated across urban and peri-urban areas, with the largest increases occurring where land cover shifted toward built-up or exposed surfaces. This spatial correspondence is consistent with an urbanization-related thermal response, but the change map alone does not establish causation because acquisition conditions and other environmental variables can also affect LST.

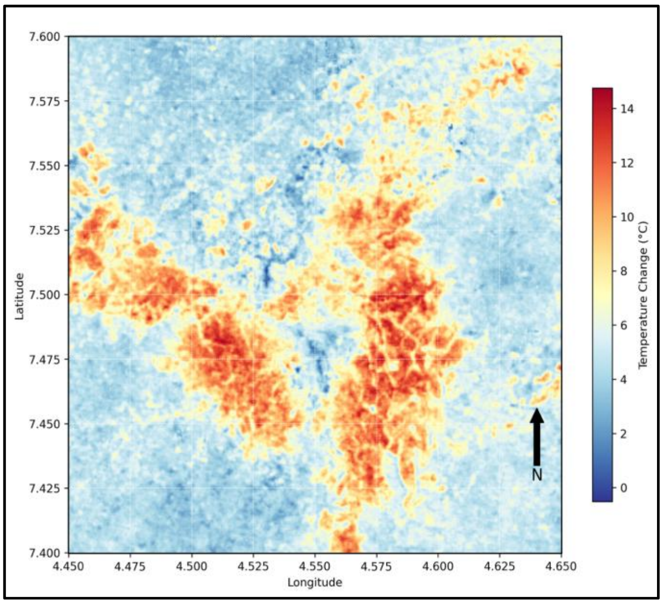

Figure 3. Change in Landsat-derived LST between 1986 and 2024.

3.2 Land-use/land-cover change

The landscape underwent marked transformation over the 38-year period (Table 4; Figure 4). Built-up land expanded by 88.07 km², from 18.20 km² in 1986 to 106.27 km² in 2024. Vegetation increased slightly between 1986 and 2002 before declining to 251.92 km² by 2024. Bare land decreased in 2002 and increased again by 2024, while mapped waterbody area remained small and declined from 0.87 km² to 0.22 km².

Table 4. LULC area comparison for Ile-Ife, 1986–2024.

Year	Vegetation (km²)	Built-Up (km²)	Waterbody (km²)	Bare Land (km²)
1986	359.52	18.20	0.87	112.93
2002	369.97	24.86	0.32	96.35
2024	251.92	106.27	0.22	133.11

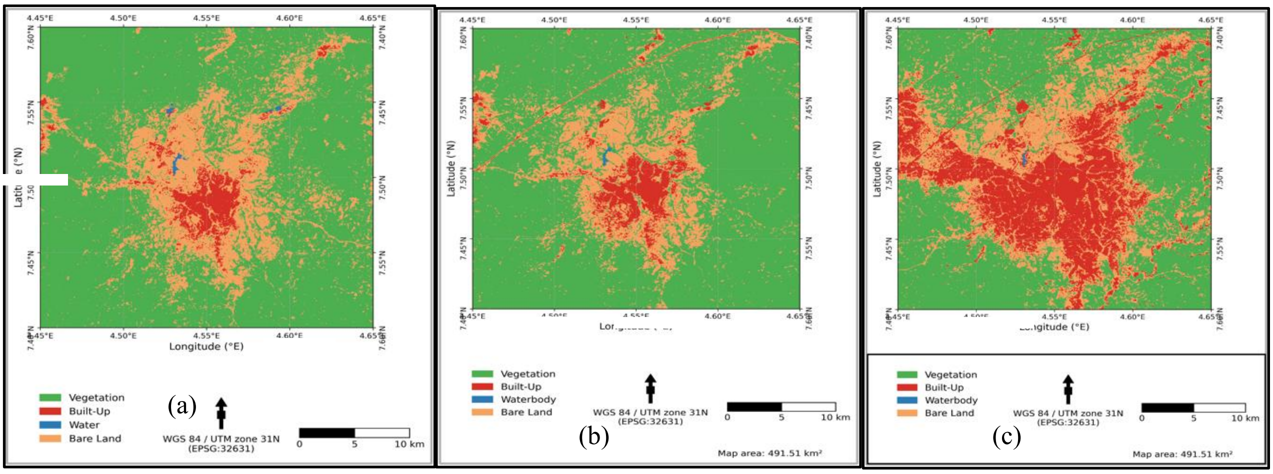

Figure 4. LULC maps for 1986 (a), 2002 (b), and 2024 (c), using a common legend and analysis boundary.

3.3 LST by land-cover class

Built-up land exhibited the highest mean LST in each benchmark year (Table 5; Figure 5): 33.35 °C in 1986, 37.90 °C in 2002, and 37.35 °C in 2024. Vegetation consistently displayed lower mean LST. The built-up–vegetation surface thermal contrast was 7.98 °C in 1986, 4.21 °C in 2002 and 7.51 °C in 2024. The smaller 2002 contrast reflects the relatively high mean vegetation temperature in that scene and should not be interpreted as a linear decline or increase in SUHI intensity.

Table 5. Mean LST by LULC type in 1986, 2002, and 2024.

LULC Type	Mean LST 1986 (°C)	Mean LST 2002 (°C)	Mean LST 2024 (°C)
Bare Land	28.13	35.76	33.08
Built-Up	33.35	37.90	37.35
Vegetation	25.37	33.69	29.84
Waterbody	28.74	34.36	29.31
Built-up–vegetation thermal contrast	7.98	4.21	7.51

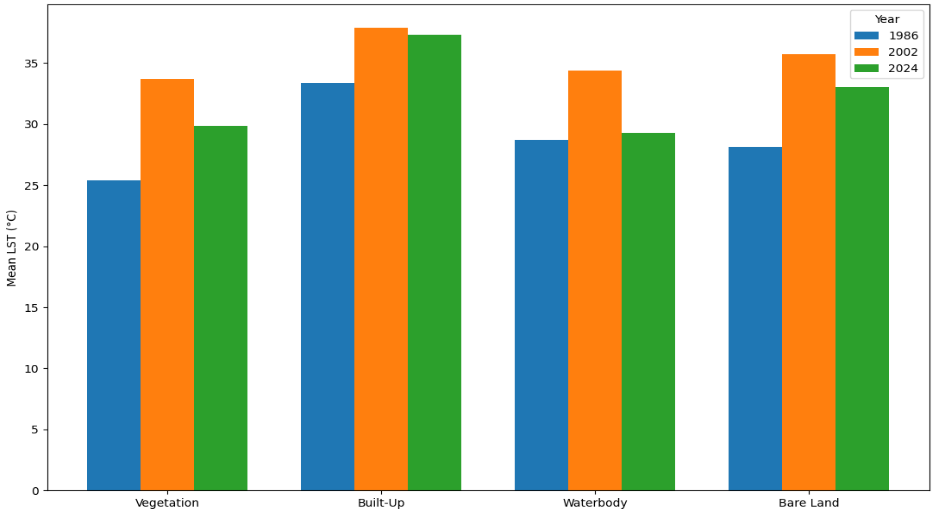

Figure 5. Mean LST by LULC type in 1986, 2002, and 2024.

3.4 Relationships of LST with NDVI and NDBI

NDVI and LST showed negative spatial associations, with r = −0.18 in 1986, −0.85 in 2002, and −0.90 in 2024. NDBI and LST showed positive associations, with r = 0.62, 0.88, and 0.90, respectively (Table 6; Figures 6 to 11). Thus, warmer pixels generally had weaker vegetation signals and stronger built-up signals, particularly in the 2002 and 2024 scenes. Because the raster values are spatially autocorrelated, the correlations are interpreted as spatial associations rather than independent causal estimates.

Table 6. Correlation of NDVI and NDBI with LST, 1986–2024.

Year	NDVI–LST r	NDVI R^2	NDBI–LST r	NDBI R^2
1986	−0.18	0.03	0.62	0.39
2002	−0.85	0.73	0.88	0.78
2024	−0.90	0.82	0.90	0.82

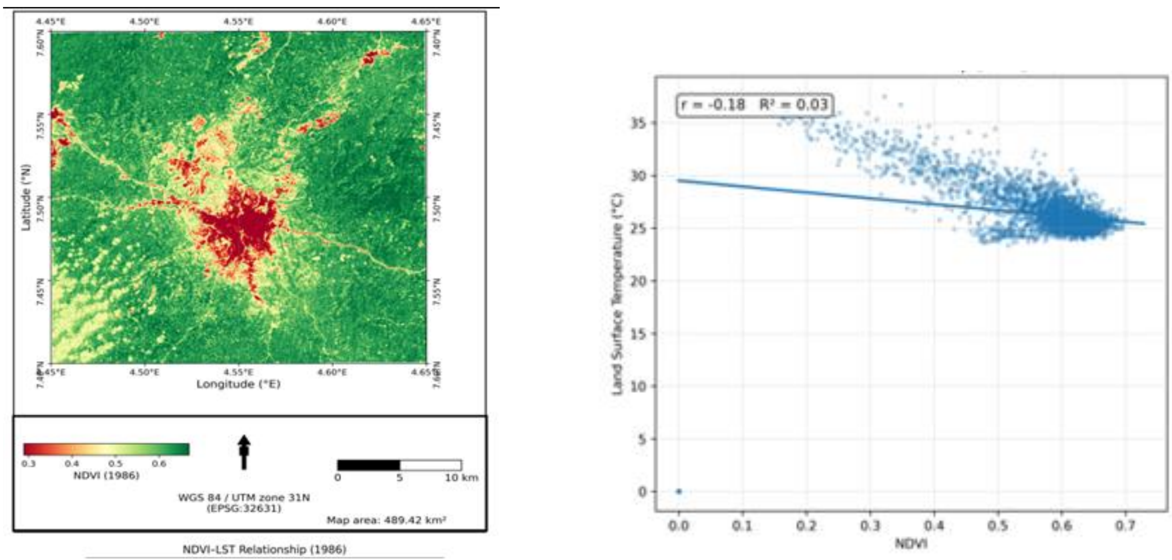

Figure 6. NDVI maps and NDVI–LST scatterplots for 1986.

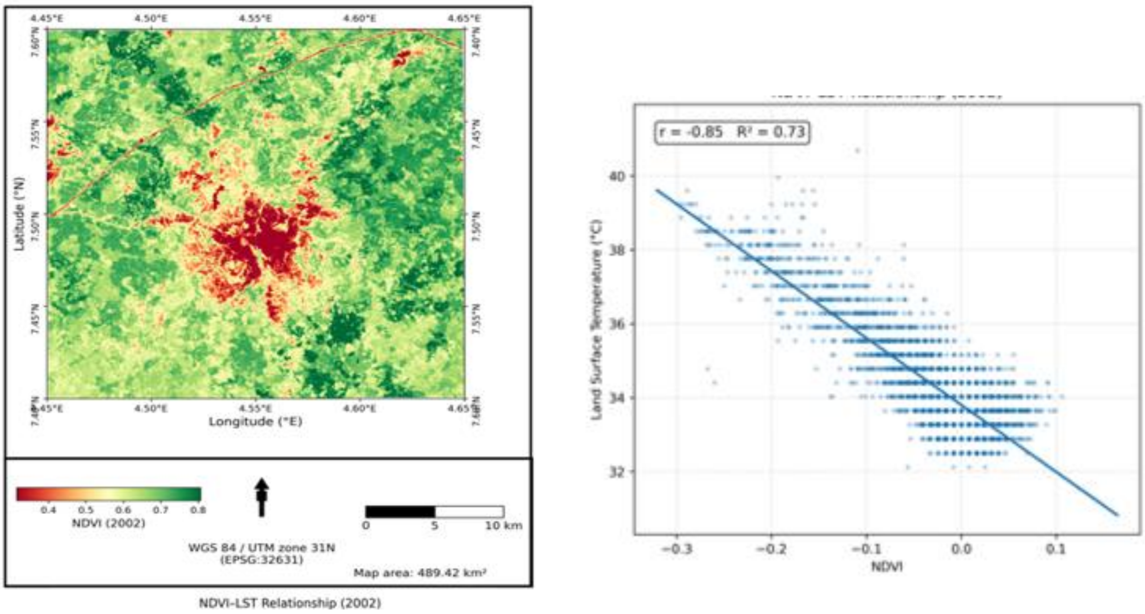

Figure 7. NDVI maps and NDVI–LST scatterplots 2002.

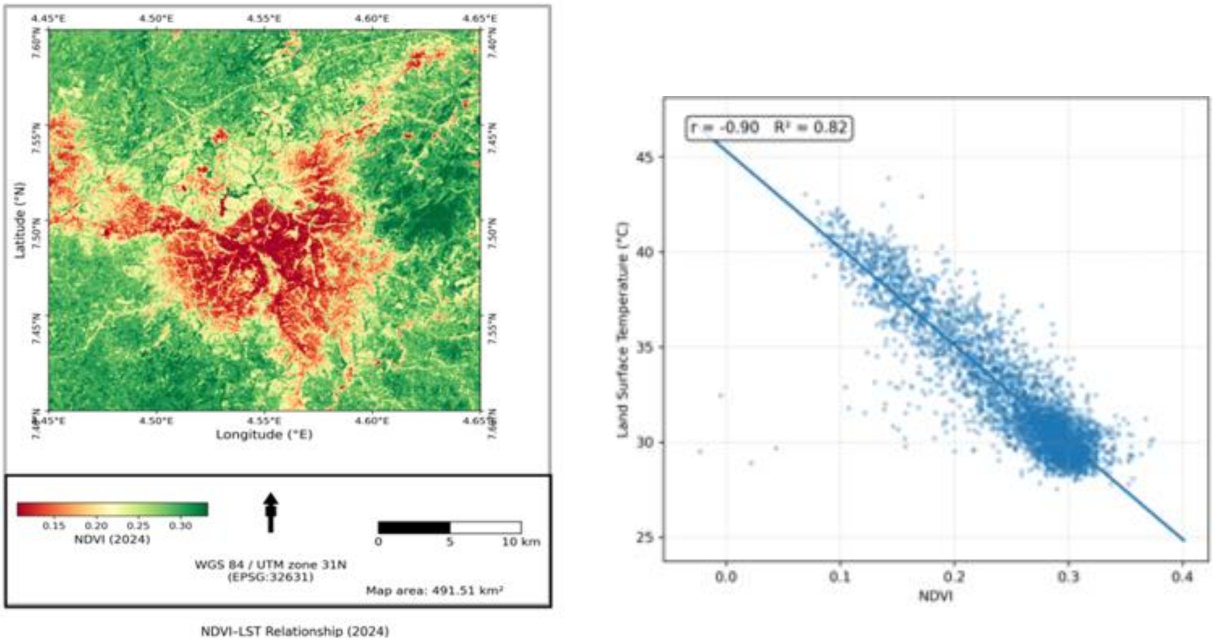

Figure 8. NDVI maps and NDVI–LS T scatterplots for 2024.

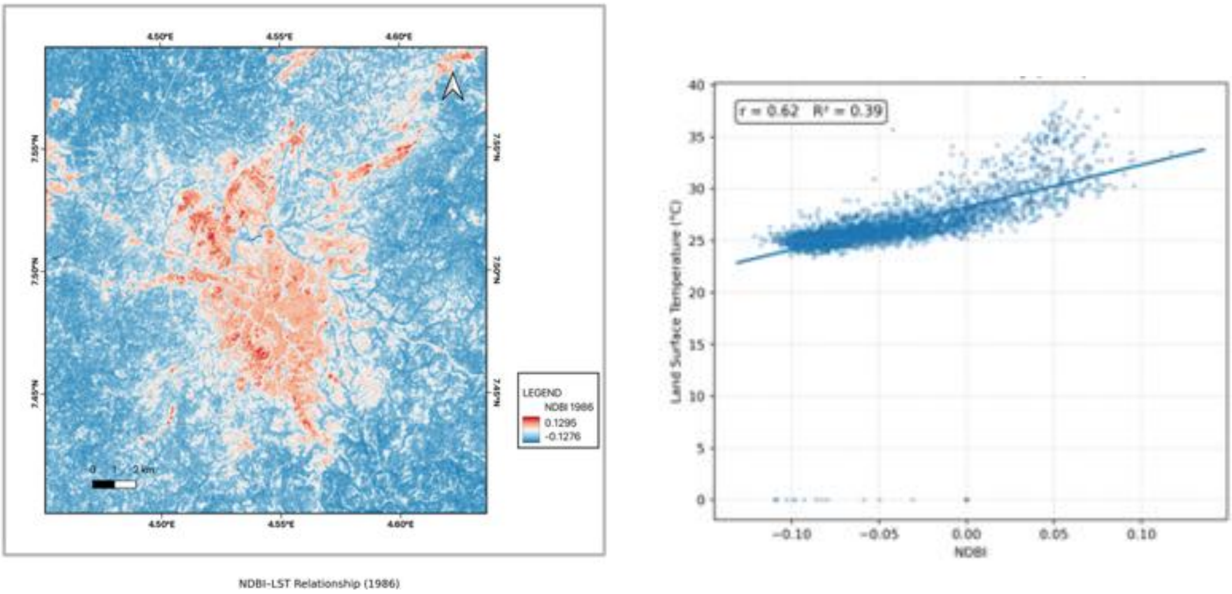

Figure 9. NDBI maps and NDBI–LST scatterplots for 1986.

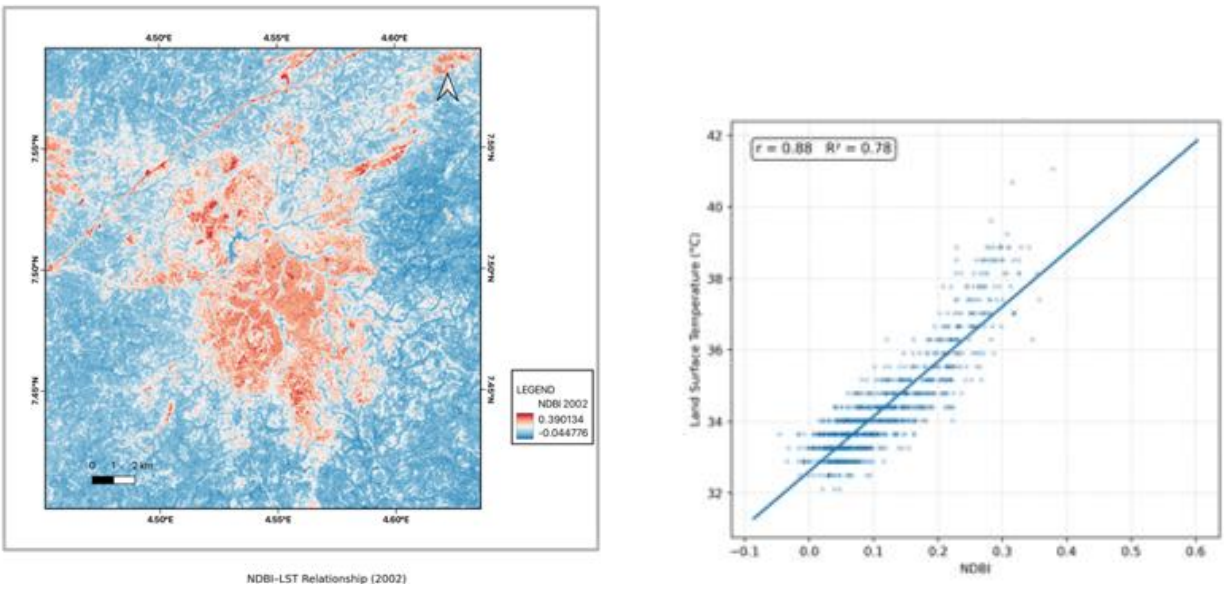

Figure 10. NDBI maps and NDBI–LST scatterplots for 2002.

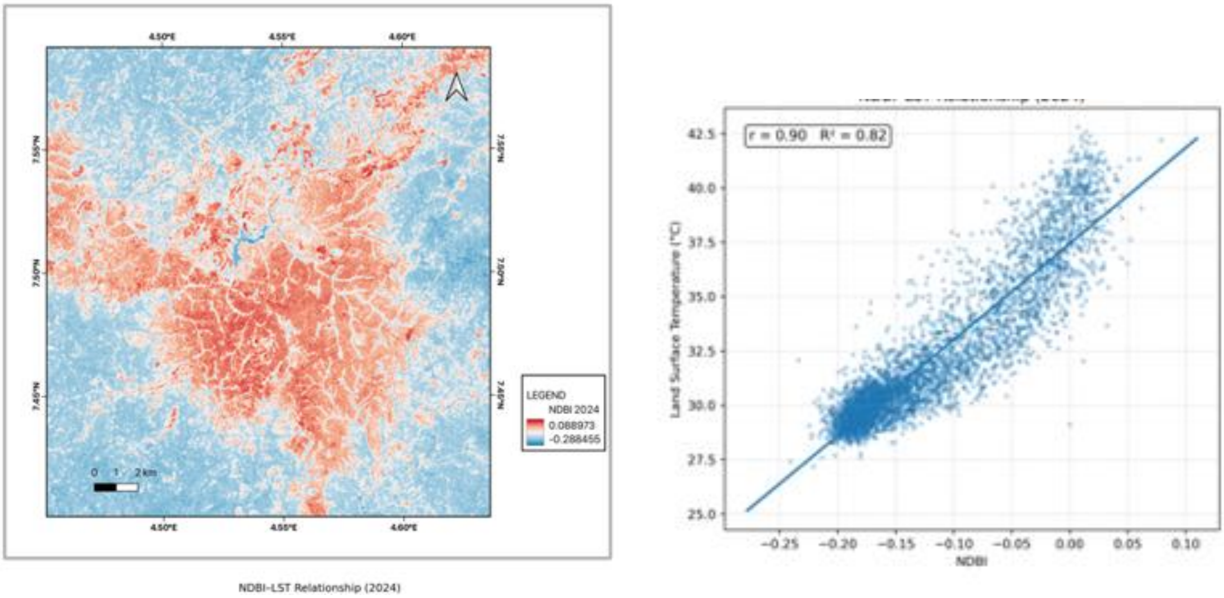

(c) 2024

Figure 11. NDBI maps and NDBI–LST scatterplots for 2024.

3.5 MODIS LST trend

The annual MODIS LST series for 2000–2024 showed a statistically significant upward trend (Figure 12). The Mann–Kendall statistic was $Z = 3.67$ with $p = 0.00025$ and Kendall's $\tau = 0.53$. Sen's slope was 0.0759 °C/year. Interannual variability remained substantial, indicating that the long-term warming trend is superimposed on shorter-term climatic and surface-moisture variability.

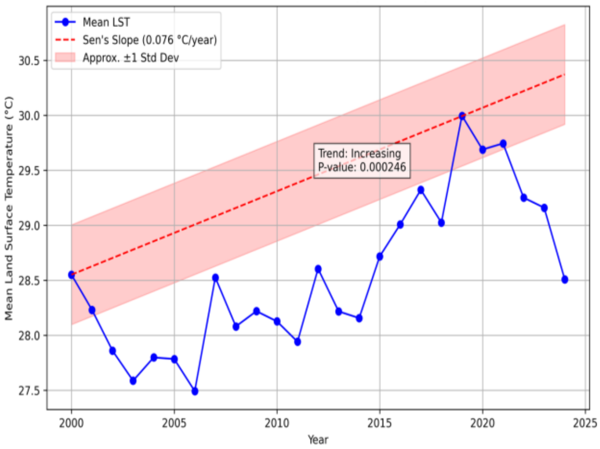

Figure 12. Annual MODIS LST for 2000–2024 with the Sen's slope trend.

3.6 Rainfall variability

CHIRPS rainfall exhibited substantial spatial and temporal variability (Table 7; Figure 13). For the three benchmark years, annual rainfall ranged from 1332.89 to 1490.32 mm in 1986, 1305.05 to 1514.56 mm in 2002, and 1512.46 to 1662.83 mm in 2024. The full series includes both comparatively dry and wet years rather than a simple monotonic pattern. Rainfall can affect LST through soil moisture, vegetation condition, cloudiness, and evapotranspiration, but these influences were not statistically isolated in the present analysis.

Table 7. CHIRPS annual rainfall statistics for benchmark years.

Year	Min Rainfall (mm/year)	Max Rainfall (mm/year)
1986	1332.89	1490.32
2002	1305.05	1514.56
2024	1512.46	1662.83

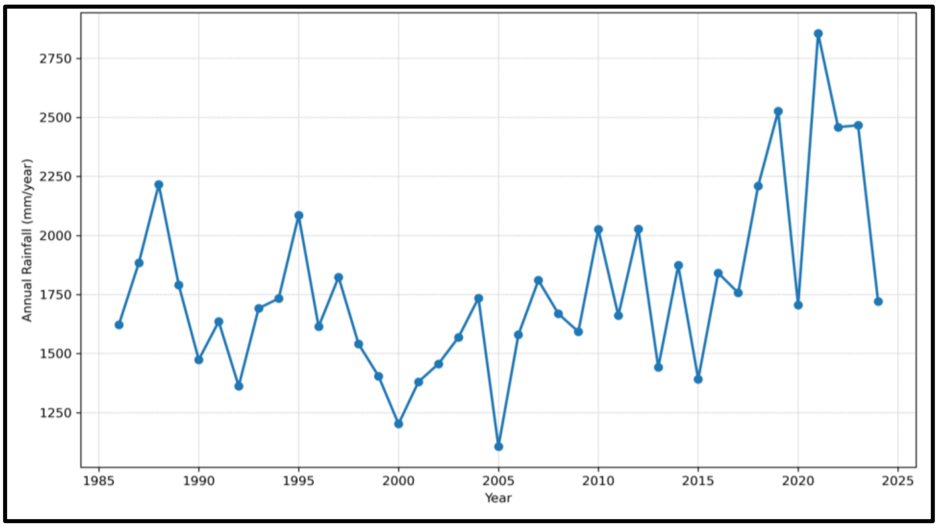

Figure 13. Annual CHIRPS rainfall for the Ile-Ife study area, 1986–2024.

4. Discussion

4.1 Urban expansion, vegetation loss, and surface warming

The clearest result is the co-location of rapid built-up expansion with warmer land surfaces. Built-up land increased from 18.20 km² to 106.27 km² between 1986 and 2024, while vegetation fell by more than 100 km². Across all three benchmark scenes, built-up surfaces had higher mean LST than vegetation. This pattern is physically consistent with the replacement of shaded, evapotranspiring surfaces by materials that store and re-radiate sensible heat. It also agrees with evidence from other tropical cities. Ayanlade (2017) reported that urban areas in Lagos were warmer than surrounding rural areas and linked the difference to dense development and limited vegetation, while Wemegah et al. (2020) found that built-up and bare surfaces in Greater Accra were most affected by urban heat-island warming.

The magnitude of the built-up–vegetation surface thermal contrast varied across scenes rather than increasing monotonically: 7.98 °C in 1986, 4.21 °C in 2002, and 7.51 °C in 2024. The smaller 2002 contrast resulted largely from a warmer vegetation class in that scene (mean vegetation LST of 33.69 °C, compared with 25.37 °C in 1986 and 29.84 °C in 2024; Table 5), rather than from a cooler built-up class. The 2002 CHIRPS record for the benchmark year was within the range observed across the three scenes (Table 7) and does not on its own indicate an unusually dry antecedent period, so the elevated vegetation temperature is more plausibly linked to the specific acquisition date, sensor, and short-term atmospheric or moisture conditions on 3 January 2002 than to a distinct climatic regime; this cannot be fully disentangled with the single-date benchmark design used here. This underscores that three single-date Landsat observations should not be treated as a direct time series of UHI intensity. Although all three scenes were acquired within a similar dry-season window, day-specific atmospheric conditions, antecedent moisture, surface condition, and sensor differences can influence absolute LST. Long-term studies elsewhere have similarly emphasized that SUHI magnitude reflects both land-cover change and background environmental conditions (Estoque & Murayama, 2017; Zhou et al., 2019).

4.2 Interpretation of NDVI and NDBI associations

The NDVI–LST and NDBI–LST relationships provide a second line of evidence linking land-surface composition to thermal patterns. NDVI became strongly negatively associated with LST in 2002 and 2024, whereas NDBI showed strong positive associations in the same scenes. These directions are consistent with the established LST–vegetation relationship reported by Weng et al. (2004) and with the broader satellite SUHI literature summarized by Zhou et al. (2019): vegetation tends to moderate surface heating through shading and evapotranspiration, while impervious and built surfaces tend to favour sensible heat storage. The strong 2024 coefficients therefore support an interpretation in which the contemporary thermal pattern of Ile-Ife is closely structured by the contrast between vegetated and developed surfaces.

These coefficients should nevertheless not be read as independent causal effect sizes. NDVI, NDBI, and LST were derived from the same raster scenes, neighbouring pixels are spatially autocorrelated, and NDVI and NDBI partly encode opposing land-cover characteristics. Accordingly, the reported r and R^2 values are best understood as descriptive spatial evidence. Future work could test the robustness of these relationships using spatial regression, stratified sampling, and multicollinearity diagnostics.

4.3 Long-term warming and rainfall context

The MODIS analysis provides temporal evidence that is not available from the three Landsat benchmark scenes. The statistically significant Sen's slope of 0.0759 °C/year corresponds to an estimated fitted increase of about 1.9 °C over 25 years if interpreted linearly. This is a trend in satellite-derived surface temperature, not a forecast and not an equivalent trend in near-surface air temperature. The result nevertheless indicates persistent warming in the surface thermal environment over the period analysed, strengthening the interpretation that the 2024 thermal pattern is part of a longer-term change rather than an isolated hot scene.

Rainfall provides important context but does not offer a simple explanation for the observed warming. The CHIRPS record was variable, and 2024 was comparatively wet within the benchmark-year ranges, yet extensive high-LST zones remained evident over developed surfaces. Background climate and moisture availability can influence urban–rural thermal contrasts through evapotranspiration and convection (Zhao et al., 2014), but the present study did not fit a model that separates rainfall from land cover, antecedent moisture, season, or atmospheric conditions. The defensible conclusion is therefore that rainfall modulates the thermal environment, while its independent contribution to the Ile-Ife trend remains unresolved.

4.4 Implications for urban planning

The spatial concentration of high LST in developed areas has practical implications for growth management in Ile-Ife. Retaining mature trees and remnant vegetation, connecting green spaces, increasing shade along streets and public facilities, and limiting unnecessary conversion of permeable land are directly aligned with the observed cooling association of vegetation. Reflective or lower-heat-storage materials may also reduce surface heating in appropriate locations, although their local performance, glare, maintenance requirements, and indoor-comfort effects should be evaluated before large-scale adoption (Akbari et al., 2009; Santamouris, 2020).

Interventions should be spatially targeted rather than uniformly applied. The thermal maps identify areas of persistent surface heating, but exposure and vulnerability were not measured in this study. Future planning analysis should therefore combine thermal hotspots with population density, housing quality, electricity access, age structure, outdoor work, health-service locations, and other locally relevant indicators before prioritizing neighbourhood-scale heat-risk interventions.

4.5 Limitations

This study has several limitations. Only three Landsat benchmark dates were used, and although all were acquired in a similar dry-season window, differences in short-term weather, atmospheric conditions, surface moisture, and sensor characteristics can influence cross-year LST comparisons. Satellite LST represents surface skin temperature and is not equivalent to near-surface air temperature or pedestrian-level thermal exposure (Voogt & Oke, 2003). Equal-interval thermal classes are useful for within-scene visualization but are not fixed SUHI thresholds that can be compared directly across years. Pixel-level Pearson correlations are affected by spatial autocorrelation and shared derivation from the same imagery and are therefore interpreted descriptively. Rainfall was evaluated as climate context, and the analysis did not estimate its independent effect after controlling for land cover, antecedent moisture, or season. LULC classification accuracy is reported with overall accuracy, Kappa, and class-level producer's and user's accuracy for all three benchmark years; minority classes with small validation samples ($n = 5–8$) nevertheless carry wide uncertainty around their class-level accuracy figures, and a larger, stratified validation dataset would tighten these estimates. Finally, night-time heat, socio-economic exposure, and neighbourhood-scale air temperature were outside the scope of the study.

5. Conclusion

This study documents substantial change in the surface thermal environment of Ile-Ife between the 1986 and 2024 benchmark scenes. Built-up land expanded from 18.20 km² to 106.27 km² while vegetation declined from 359.52 km² to 251.92 km². Built-up surfaces were warmer than vegetation in every benchmark year, and the 2024 scene showed a built-up–vegetation surface thermal contrast of 7.51 °C. NDVI was strongly negatively associated with LST in 2024 ($r = −0.90$), whereas NDBI was strongly positively associated with LST ($r = 0.90$). The independent MODIS time series also showed a significant long-term surface warming trend from 2000 to 2024 ($Z = 3.67$, $p = 0.00025$; Sen’s slope = 0.0759 °C/year). Taken together, the land-cover, spectral-index, and trend evidence is consistent with rapid urban expansion and vegetation loss contributing substantially to surface warming in Ile-Ife. The analysis does not, however, isolate a single causal driver, and rainfall, surface moisture, atmospheric variability, and sensor differences remain relevant sources of variation.

For planning, the findings support protection and expansion of urban vegetation, retention of permeable surfaces, and targeted heat-sensitive design in rapidly developing areas. Future work should include more Landsat dates, spatial statistical models, larger and stratified validation samples for minority land-cover classes, night-time or near-surface air-temperature observations, and socio-economic exposure data so that surface thermal hotspots can be translated into a more complete assessment of urban heat risk.

Acknowledgement

The author acknowledges the African Regional Institute for Geospatial Information Science and Technology (AFRIGIST) and the Federal University of Technology, Akure (FUTA), for institutional and supervisory support. The author also acknowledges USGS, NASA LP DAAC, and the Climate Hazards Center for access to the satellite and rainfall datasets used in the study.

Conflict of Interest

The author declares no conflict of interest, financial or otherwise, that could have influenced the design, analysis, interpretation, or reporting of this study.

Originality

This manuscript is the author's original work, has not been published elsewhere, and is not under consideration for publication in any other journal or outlet. All data sources and prior work used in this study have been appropriately cited.

References

Akbari, H., Menon, S., & Rosenfeld, A. (2009). Global cooling: Increasing world-wide urban albedos to offset CO_2. Climatic Change, 94(3–4), 275–286. https://doi.org/10.1007/s10584-008-9515-9

Ayanlade, A. (2017). Variations in urban surface temperature: An assessment of land use change impacts over Lagos metropolis. Weather, 72(10), 315–319. https://doi.org/10.1002/wea.2925

Chander, G., Markham, B. L., & Helder, D. L. (2009). Summary of current radiometric calibration coefficients for Landsat MSS, TM, ETM+, and EO-1 ALI sensors. Remote Sensing of Environment, 113(5), 893–903. https://doi.org/10.1016/j.rse.2009.01.007

Congalton, R. G., & Green, K. (2019). Assessing the accuracy of remotely sensed data: Principles and practices (3rd ed.). CRC Press.

Estoque, R. C., & Murayama, Y. (2017). Monitoring surface urban heat island formation in a tropical mountain city using Landsat data (1987–2015). ISPRS Journal of Photogrammetry and Remote Sensing, 133, 18–29. https://doi.org/10.1016/j.isprsjprs.2017.09.008

Mann, H. B. (1945). Nonparametric tests against trend. Econometrica, 13(3), 245–259.

Santamouris, M. (2020). Recent progress on urban overheating and heat island research: Integrated assessment of the energy, environmental, vulnerability and health impact; synergies with global climate change. Energy and Buildings, 207, 109482. https://doi.org/10.1016/j.enbuild.2019.109482

Sen, P. K. (1968). Estimates of the regression coefficient based on Kendall’s tau. Journal of the American Statistical Association, 63(324), 1379–1389. https://doi.org/10.1080/01621459.1968.10480934

Tucker, C. J. (1979). Red and photographic infrared linear combinations for monitoring vegetation. Remote Sensing of Environment, 8(2), 127–150. https://doi.org/10.1016/0034-4257(79)90013-0

United Nations, Department of Economic and Social Affairs, Population Division. (2019). World Urbanization Prospects: The 2018 Revision (ST/ESA/SER.A/420). United Nations.

Vermote, E., Justice, C., Claverie, M., & Franch, B. (2016). Preliminary analysis of the performance of the Landsat 8/OLI land surface reflectance product. Remote Sensing of Environment, 185, 46–56. https://doi.org/10.1016/j.rse.2016.04.008

Voogt, J. A., & Oke, T. R. (2003). Thermal remote sensing of urban climates. Remote Sensing of Environment, 86(3), 370–384. https://doi.org/10.1016/S0034-4257(03)00079-8

Wemegah, C. S., Yamba, E. I., Aryee, J. N. A., Sam, F., & Amekudzi, L. K. (2020). Assessment of urban heat island warming in the Greater Accra Region. Scientific African, 8, e00426. https://doi.org/10.1016/j.sciaf.2020.e00426

Weng, Q., Lu, D., & Schubring, J. (2004). Estimation of land surface temperature–vegetation abundance relationship for urban heat island studies. Remote Sensing of Environment, 89(4), 467–483. https://doi.org/10.1016/j.rse.2003.11.005

Zha, Y., Gao, J., & Ni, S. (2003). Use of normalized difference built-up index in automatically mapping urban areas from TM imagery. International Journal of Remote Sensing, 24(3), 583–594. https://doi.org/10.1080/01431160304987

Zhao, L., Lee, X., Smith, R. B., & Oleson, K. (2014). Strong contributions of local background climate to urban heat islands. Nature, 511, 216–219. https://doi.org/10.1038/nature13462

Zhou, D., Xiao, J., Bonafoni, S., Berger, C., Deilami, K., Zhou, Y., Frolking, S., Yao, R., Qiao, Z., & Sobrino, J. A. (2019). Satellite remote sensing of surface urban heat islands: Progress, challenges, and perspectives. Remote Sensing, 11(1), 48. https://doi.org/10.3390/rs11010048